Scripta Materialia 126 (2017) 50–54

Contents lists available at ScienceDirect

Scripta Materialia

journal homepage: www.elsevier.com/locate/scriptamat

Regular Article

Atomically resolved chemical ordering at the nm-thick TiO precipitate/matrix interface in V-4Ti-4Cr alloy

A. Impagnatiello [a,b,*], D. Hernandez-Maldonado [c], G. Bertali [b], E. Prestat [b], D. Kepaptsoglou [c], Q. Ramasse [c], S.J. Haigh [b], E. Jimenez-Melero [a,b]

[a] Dalton Cumbrian Facility, The University of Manchester, Moor Row CA24 3HA, UK
[b] School of Materials, The University of Manchester, Manchester M13 9PL, UK
[c] SuperSTEM Laboratory, STFC Daresbury Campus, Keckwick Lane, Daresbury WA4 4AD, UK

ARTICLE INFO

Article history:
Received 20 June 2016
Received in revised form 29 July 2016
Accepted 18 August 2016
Available online xxxx

Keywords:
Refractory metal
Crystalline oxides
Lattice defects
High-resolution electron microscopy
Nuclear fusion reactor

ABSTRACT

We have used advanced analytical electron microscopy to characterise the local structure and chemistry at the interface between nm-thick TiO precipitates and the V-based matrix in a V-4Ti-4Cr alloy. Our results reveal the presence of an intergrowth between the fcc TiO and bcc vanadium structures, with a repeat lattice distance that equals 2.5 times the vanadium lattice parameter along the c-axis. Our atomic resolution analysis of the interface will impact the mechanistic understanding of its interaction with interstitials and radiation-induced lattice defects, and consequently trigger the development of improved alloy structures with interfaces engineered for enhanced radiation tolerance.

Vanadium-based alloys constitute advanced structural material candidates for the first wall of future magnetically-confined fusion reactors, due to their relatively low cross section for neutron activation [1,2]. Consequently, the targeted tritium breeding ratio will be achieved without the need of an additional neutron-multiplier material such as beryllium. The high strength and creep resistance of V-based alloys, enhanced by the addition of Cr, will allow these materials to withstand temperatures up to 750 °C without compromising reactor operability and safety [3]. In addition, the body-centred cubic (bcc) nature of the V matrix, with additions of Ti, provides these materials with good resistance to radiation-induced void swelling [4,5]. These considerations have led to the V-4Cr-4Ti alloy being identified as the prime V-based candidate material for fusion reactor applications [2,6,7].

However, the presence of H, C, O and N as 'free interstitials' in the V-matrix causes the detrimental shift of the ductile-to-brittle transition temperature from −200 °C to values well above room temperature [8–10]. Ti was identified as an effective scavenger for interstitials [11], by forming plate-like oxycarbo-nitride precipitates [12–15]. The additional benefit is that the precipitate/matrix interface could potentially act as an effective sink for radiation-induced lattice defects, such as vacancies, vacancy clusters or dislocation loops, or for transmutant helium atoms [16,17]. Unfortunately, a unified view about the local structure and chemistry of these nano-precipitates is still lacking. In this paper, we have addressed this by characterising, with atomic resolution, the chemical distribution and local structure inside the precipitates and within the precipitate-matrix interface region.

In this study we annealed V-4Cr-4Ti (wt.%) sheet material for 2 h at 1200 °C in an inert atmosphere, followed by water-quenching to room temperature. For transmission electron microscope (TEM) imaging and analysis discs were prepared by mechanical pre-thinning, followed by electro-polishing using an electrolyte of 60 vol.% methanol–35 vol.% 2-buthoxyethanol–5 vol.% perchloric acid (60%) at a temperature of −35 °C. Advanced scanning transmission electron microscope (STEM) imaging, coupled with Energy-dispersive X-ray Spectroscopy (EDS) and Electron Energy Loss Spectroscopy (EELS) measurements performed in a STEM microscope, was used to obtain structural and chemical information with atomic resolution. A High Angle Annular Dark Field (HAADF) detector was used to collect the Rutherford-like scattering signal while the subnanometre-sized electron probe was scanning the sample. The intensity in the HAADF images is proportional to Z^{ν}, where Z denotes the atomic number and $\nu = 1.6–1.9$ [18]. The HAADF data therefore yielded information about the atomic positions and local arrangements inside the Ti-rich precipitates present in the V-4Cr-4Ti alloy. For the chemical identification we used (1) STEM-EDS to detect elements with high atomic number, and (2) STEM-EELS suitable to detect low-Z elements, and also to determine the chemical environment of a specific element.

* Corresponding author at: Dalton Cumbrian Facility, University of Manchester, Westlakes Science & Technology Park, Moor Row CA24 3HA, UK.
E-mail address: andrea.impagnatiello@postgrad.manchester.ac.uk (A. Impagnatiello).

http://dx.doi.org/10.1016/j.scriptamat.2016.08.016
1359-6462/

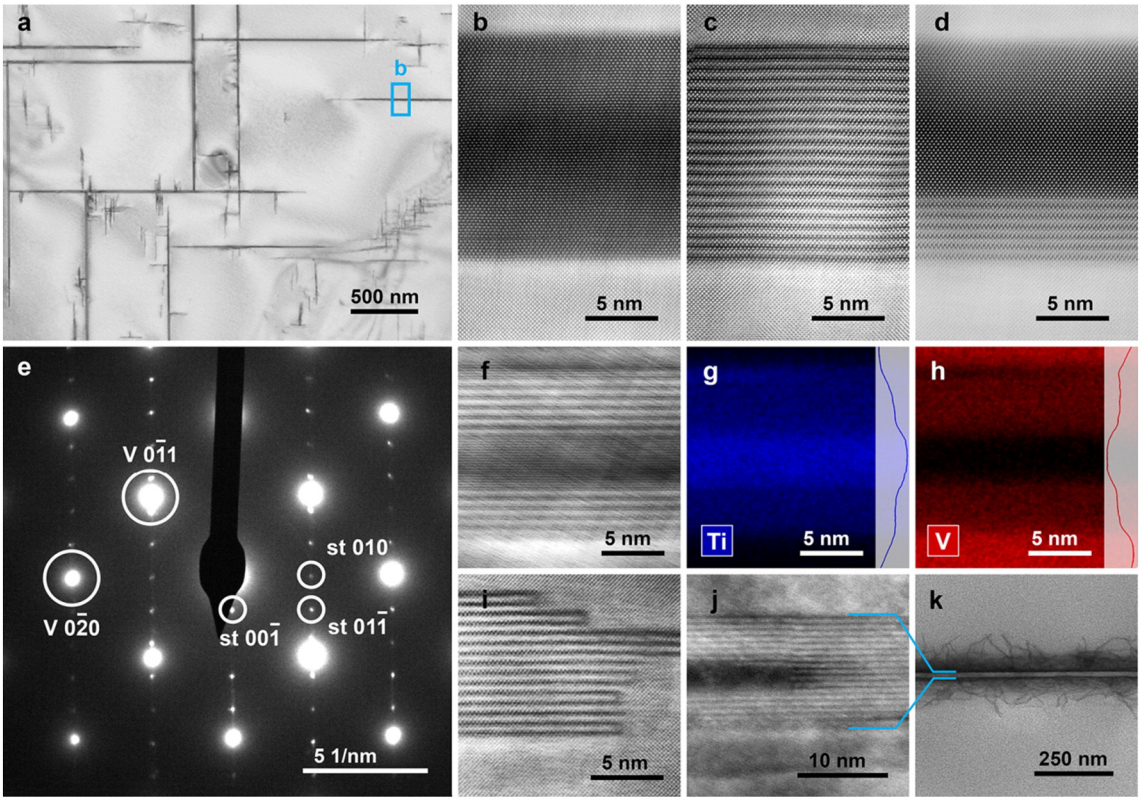

Fig. 1. (a) TEM BF image of the V-4Ti-4Cr alloy microstructure with the plate-like precipitates viewed along the [001] zone axis. (b–d) HAADF images showing precipitates with (b) a uniform atomic structure, (c) a superstructure and (d) both uniform and superstructure regions. (e) The corresponding SADP of (a) with the V matrix and simple tetragonal (st) superstructure reflections highlighted. Precipitates with different proportions of superstructure fringes: (f) with superstructure at both long sides with the relative EDS spectrum images for (g) K_α Ti and (h) K_α V, (i) with superstructure at the short edge of the precipitates, and (j) with superstructure surrounding a region of uniform atomic structure. (k) BF image of a precipitate with dislocations pinned at the precipitate-matrix interface.

Fig. 1a shows a TEM bright-field (BF) image of the V-4Cr-4Ti specimen after the annealing treatment. A significant number of plate-like precipitates, with lengths of up to a few microns and only a few tens of nanometres in width, were observed in this material. The selected area electron diffraction pattern (SADP) in Fig. 1e shows the [001] zone axis of the V matrix with additional reflections due to the presence of one of the plate-like precipitates. The lattice parameter of bcc V (a_v) is ~3.02 Å. The pattern clearly shows that the plates are lying on the V{100} family of planes. Additionally, we have observed the presence of diffraction spots corresponding to a superstructure with a spacing of ~7.56 Å, which corresponds to ~2.5 times the lattice parameter of the matrix.

High resolution STEM imaging of the precipitates (Fig. 1) revealed a range of atomic structures within different plate-like precipitates: uniform (b), showing a superstructure through the thickness (c), or showing a superstructure localised on one (d) or both (f) long sides of the precipitates. The spacing determined in the high resolution STEM data for the superstructure corresponds to the value obtained from the SADP. Fig. 1g and h are the related background-subtracted EDS spectrum images for the Kα Ti and Kα V lines, respectively. The EDS data show that the uniform area of the precipitate mainly contains Ti, whereas both Ti and V are present in the superstructure regions. Cr has not been detected in significant amounts inside any of the precipitates. Two additional cases are also reported in Fig. 1: superstructure at the short edge of the precipitates (i), and surrounding a region of uniform atomic structure (j). Interestingly, the interface between the precipitate superstructure and the matrix acts as an effective trap for dislocations present in the matrix (k).

In order to obtain further information about the local chemical distribution and the origin of the interfacial superstructure phase, we recorded the EELS core loss and low loss spectra [19] at representative locations of the matrix, the superstructure and the uniform structure of the precipitate (Fig. 2). The EELS core loss spectrum of the matrix is dominated by the $L_{2,3}$ edges of vanadium (in the region of 440–590 eV). A relatively weak $L_{2,3}$ edge from the substitutional Cr atoms can also be observed close to 580 eV. When profiling from the matrix to the superstructure of the precipitate, the vanadium edge is still visible but decreases in intensity, whereas the $L_{2,3}$ edge of Ti starts to appear at characteristic peak energies of 457 and 462 eV. The edge consists of L_3 and L_2 'white lines' which originate from electron transitions from the inner $2p_{3/2}$ and $2p_{1/2}$ orbitals respectively to empty 3d orbitals of Ti [20]. Those characteristic Ti lines constitute the main feature of the EELS spectrum in the uniform structure of the precipitate. Additionally, we can also observe the appearance of the K-edge of oxygen at 530-550 eV, with the most distinctive maximum located just above the edge onset at 532 eV. The lower-energy features of this peak are known to originate from transitions between oxygen 1 s and 2p σ^* states that are hybridised with empty Ti 3d orbitals [20]. The intensity of the 532 eV peak increases when moving the beam from the matrix into the superstructure and further into the uniform structure of the precipitate. We have not observed any significant signal in the EELS spectrum at around 280 and 400 eV which suggests the absence of C or N within the precipitate. These results would point to the precipitates consisting of a titanium oxide phase. To confirm this, we have also examined the EELS low loss or valence spectrum below 35 eV (Fig. 2c), which is dominated by plasmon excitations. The main plasmon peak of the matrix at 21.6(1) eV can be attributed to metallic vanadium [19]. The position of the maximum consistently shifts to a value of 23.8(1)eV inside the precipitate. An equivalent peak shift is observed for the superstructure and the uniform structure in the precipitate, see Fig. 2a-II. The main plasmon peak of metallic Ti would be located at 18 eV [19], and is expected to shift to ~20 eV when forming Ti hydrides

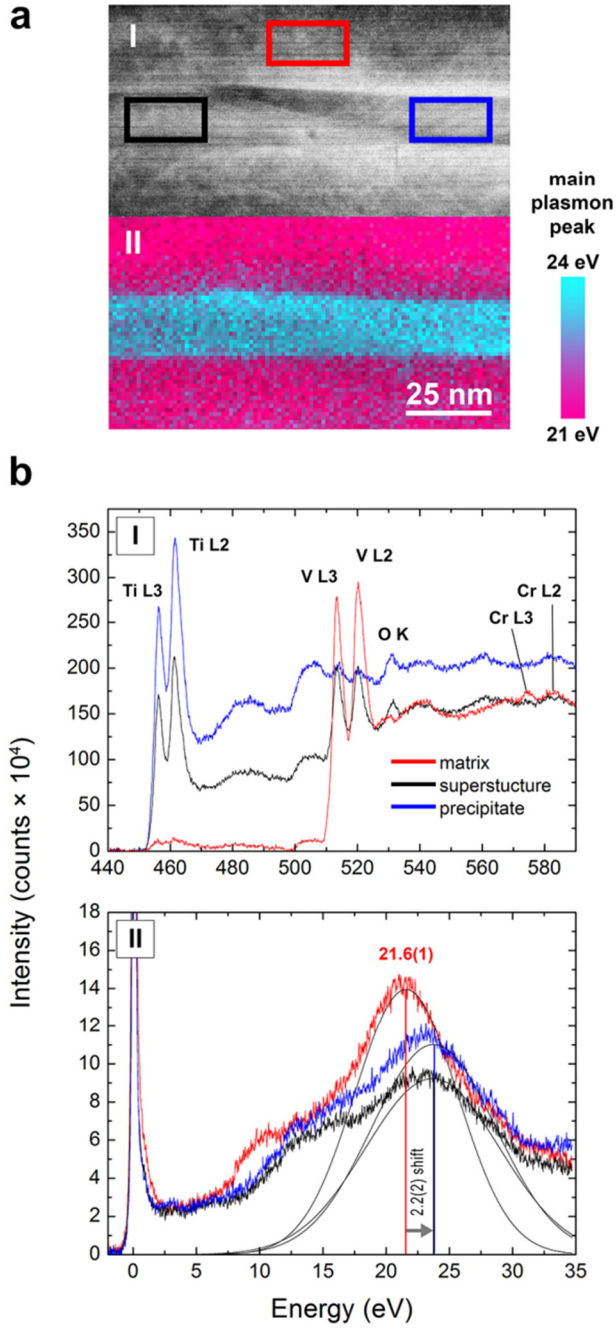

Fig. 2. (a-I) HAADF image showing a precipitate with regions of both uniform structure and superstructure and (a-II) related map of the plasmon peak. (b-I) EELS core loss and (b-II) EELS low loss spectra taken from the regions highlighted by the coloured squares in (a-I), corresponding to matrix (red), superstructure (black) and uniform precipitate (blue) structure regions. The fitted position of the main plasmon peak in the region of interest is reported in (a-II). (For interpretation of the references to colour in this figure legend, the reader is referred to the web version of this article.)

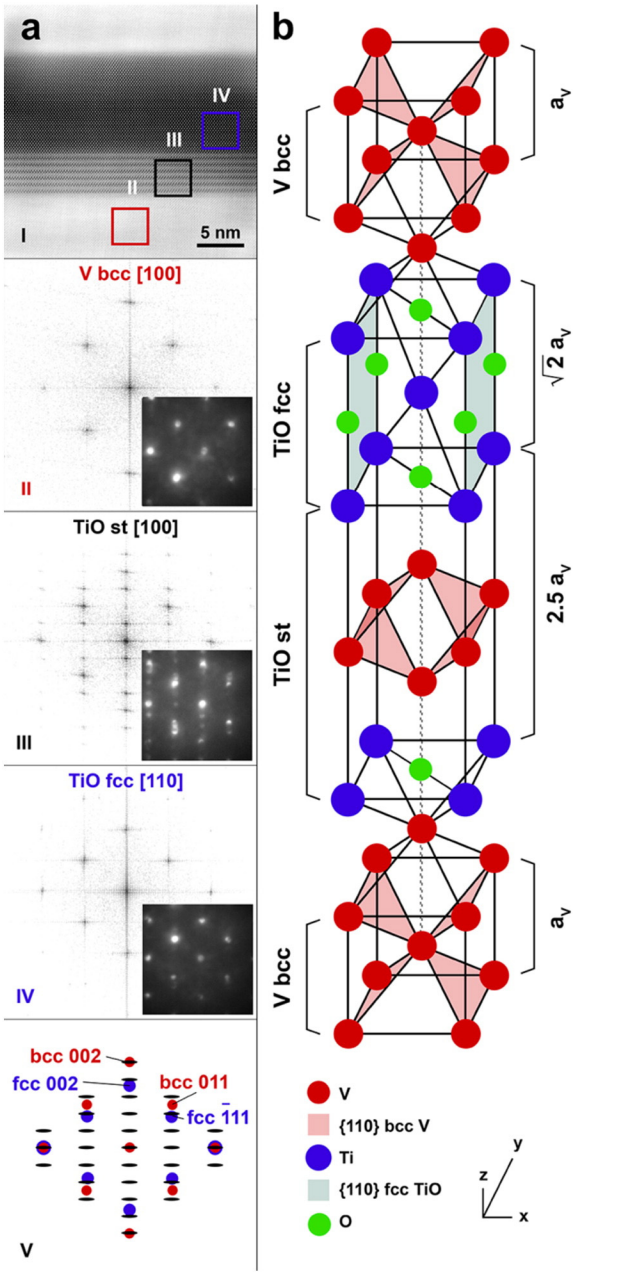

Fig. 3. (a-I) HAADF image showing a TiO precipitate with regions of both superstructure and uniform atomic structure. (a-II) to (a-IV) show the FFT and diffraction patterns taken from the regions outlined by the coloured squares in (a-I). (a-V) is the superimposed pattern containing the position of the spots in (a-II) to (a-IV). (b) Proposed crystal structure model relating the V bcc matrix structure to the TiO fcc (NaCl-type) precipitate and the superstructure (simple tetragonal 'st' of TiO with V). The lattice parameter of both TiO structures is indicated taking the lattice parameter (a_V) of the V bcc matrix as reference. (For interpretation of the references to colour in this figure legend, the reader is referred to the web version of this article.)

[21] and to 22–26 eV when Ti forms compounds with C, N or O [19,20]. Our combined EELS core loss and low loss spectral data are therefore consistent with a titanium oxide phase as precipitate.

An HAADF image of one of the precipitates and surrounding matrix is shown in Fig. 3a, together with its Fast Fourier Transform (FFT) and the measured electron diffraction pattern taken at selected locations in the precipitate and the matrix. The diffraction pattern of the matrix corresponds to the vanadium bcc structure acquired along the [100] zone axis. The pattern of the uniform structure in the precipitate has been indexed based on a face-centred cubic TiO unit cell (S.G. Fm-3m) along the [110] zone axis. This titanium mono-oxide phase presents a NaCl-type fcc structure, with a reported value of its lattice parameter of 4.184 Å. Its structure can host up to approx. 15% of vacancies [22,23], and also small amounts of C and N, since both TiN and TiC are isostructural with TiO [24]. We have determined the lattice parameter of the TiO-type precipitates in V-4Cr-4Ti as 4.28 Å. This value corresponds to $\sqrt{2}\,a_V$, where a_V is the lattice parameter of V matrix. Furthermore, the TiO precipitates must be related to the V matrix by the Baker–Nutting orientation relationship: $[001]_{TiO}$ // $[001]_V$, $(110)_{TiO}$ // $(100)_V$. From these results, it is then possible to construct a proposed model for the

superstructure in the precipitates, which consists of an intergrowth of the two end structures: the 'V bcc matrix' and the 'TiO fcc uniform structure', see Fig. 3b. The unit cell contains one vanadium octahedron from the V bcc structure, located between two 'TiO layers'. The unit cell becomes elongated along the c-axis with a lattice parameter of $c = 2.5 \times a_V \sim 7.56$ Å. The orientation relationship of the superstructure with the V matrix is thus: $[001]_{st}$ // $[001]_V$, $(100)_{st}$ // $(100)_V$.

Fig. 4 contains a plan view representation of the proposed model along the [100] direction, together with an experimental atomic resolution HAADF image of the superstructure, and the spatial distribution of the V and Ti derived from the EELS spectra using the $L_{2,3}$ edges of both elements. The combined interpretation of the chemical and structural data strongly supports the validity of the proposed superstructure model. The repeat distance of ~7.56 Å corresponds to the *c*-axis of the simple tetragonal unit cell. The dark and bright lines observed in the HAADF images can therefore be linked to TiO and V layers respectively. Careful examination and comparison of the images and chemical information from the EELS data also suggest that it is possible to identify individual V atoms at two positions in the unit cell, i.e. $x = 0$ and $x = 1/2$ from the V octahedron in the intergrowth, and also interleaving Ti atoms.

Some simple diffusion considerations can be put forward to explain how the superstructure forms. When the sample is annealed at 1200 °C, both Ti and O diffuse in the V bcc matrix to form the TiO precipitates. The diffusion of O interstitials is relatively fast; with a reported value of the activation energy of 119.6–122.5 kJ mol^{-1} [25–27]. Early trace diffusion experiments in binary V-Ti alloys yielded a value for the Ti diffusion coefficient of ~1.5×10^{-3} $\mu m^2/s$ at 1200 °C [28]. If we assume a random walk approach for the diffusion of Ti in the V matrix, we obtain a Ti diffusion length of $\sqrt{Dt} \sim 3.3$ μm. This value is in good agreement with our experimental value for the average precipitate length in this material (≈3 μm). A correlation factor (f) is defined as the ratio of the diffusion coefficient of a given species, Ti in this case, to the diffusion coefficient calculated assuming randomly oriented jump vectors [29]. The reported value of this correlation value for Ti diffusion, assuming that the Ti atoms produce only a weak perturbation of the V lattice and also a vacancy-mediated mechanism, takes a value lower than but close to 1, i.e. $f_{Ti} = 0.75$–0.80 in the temperature range of 1100–1550 °C [28]. In general, the greater the freedom of movement of the vacancy, the less important the correlation effects become, and therefore the smaller 1-f is [30]. This means that the binding energy for a Ti-vacancy is relatively low, and the random walk treatment is a suitable approach for the Ti diffusion in the V matrix. The V self-diffusion is slower than the Ti diffusion, but the V diffusivity is affected by the rate at which Ti-vacancy pairs break up. The V diffusion coefficient takes a value of ~6.0×10^{-4} $\mu m^2/s$ at 1200 °C [28,31], which yields a V diffusion length of $\sqrt{Dt} \sim 2.1$ μm. V can therefore form the superstructure phase together with Ti along the precipitate-matrix interface during the annealing treatment.

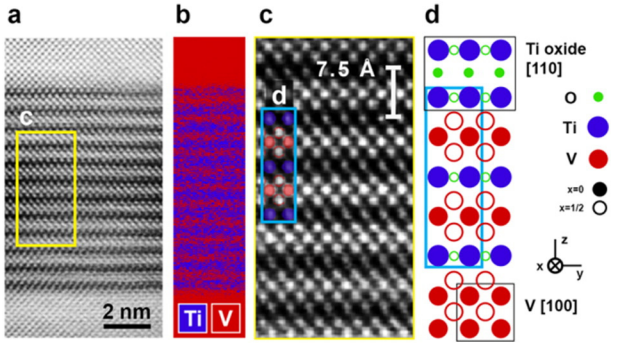

Fig. 4. (a) HAADF image of the superstructure within the precipitate, (b) composite image constructed from the EELS maps generated by integrating the $L_{2,3}$ edge intensity of V (red) and Ti (blue). (c) Atomic resolution detail of the region marked by the yellow rectangle in (a), with atomic positions superimposed inside the blue rectangle. (d) Crystal structure model showing two repeating units of the superstructure along the *z*-direction with the atomic pattern shown in (c) highlighted by the blue rectangle. (For interpretation of the references to colour in this figure legend, the reader is referred to the web version of this article.)

The local structure and chemical distribution at the precipitate interface with the V matrix will influence the strength of the precipitates as sinks and recombination sites for radiation-induced lattice defects and He atoms [32]. Helium has a relatively low solubility in metals [33,34], and hence the diffusion and accumulation of He at interfaces and grain boundaries can potentially form bubbles. The presence of He has also been proposed to accelerate the radiation-induced swelling, both by stabilising the void nuclei formed by clustering of the vacancy defects, and by enhancing the void growth that may lead to percolating networks [35]. The leading approach to mitigating void swelling in He-containing materials is to delay the bubble transformation into voids by nano-structuring [36,37]. Recent work reports the role of semi-coherent fcc-bcc heterophase interfaces in delaying bubble growth in nano-layered composites, materials in which helium seems to accumulate at intersections between misfit dislocations. The spacing between those dislocation interactions could therefore be optimised to influence the effectiveness of the interface as point defect sinks so that enhanced damage tolerance is achieved [35,38]. In the case of the TiO(fcc)-V(bcc) system, the observed atomic ordering at the interface could effectively delay the He bubble growth, and also accommodate significant amounts of lattice defects and interstitial atoms at the interface, so that low-temperature embrittlement is minimised or delayed.

In conclusion, our atomic-resolution STEM imaging and analysis results have revealed the presence of an intergrowth of the TiO fcc and V bcc structures at the precipitate/matrix interface in the V-4Ti-4Cr alloy. The O atoms are primarily concentrated inside the nm-thick precipitates, where they seem to be homogeneously distributed, while the V/Ti superstructure atomic ordering can in some cases extend through the full thickness of the plate-like precipitates. This atomic-scale characterisation of the local structure and chemistry of the interface and precipitate structure will assist the mechanistic understanding of the interaction of interstitials and radiation-induced lattice defects with the precipitate interface, and hopefully trigger the development of novel alloy structures with enhanced radiation tolerance.

We acknowledge the Engineering and Physical Sciences Research Council (EPRSC) for providing funding for this project via the Centre for Doctoral Training in the Science and Technology of Fusion Energy (http://www.fusion-cdt.ac.uk/), and also for providing access to the SuperSTEM Laboratory, the U.K. National Facility for Aberration-Corrected STEM (http://www.superstem.com/). S.J.H. would like to acknowledge the EPSRC grant EP/M010619/1 as well as the Defence Threat Reduction Agency grant number HDTRA1-12-1-0013. We would also like to thank Matthew Smith for his valuable help with the FEI Titan microscope in Manchester.

Appendix A. Supplementary data

Supplementary data to this article can be found online at http://dx.doi.org/10.1016/j.scriptamat.2016.08.016.

References

[1] S.J. Zinkle, A. Möslang, T. Muroga, H. Tanigawa, Nucl. Fusion 53 (2013) 104024.
[2] T. Muroga, J.M. Chen, V.M. Chernov, R.J. Kurtz, M. Le Flem, J. Nucl. Mater. 455 (2014) 263.
[3] S.J. Zinkle, N.M. Ghoniem, Fusion Eng. Des. 51–52 (2000) 55.
[4] B.A. Loomis, D.L. Smith, F.A. Garner, J. Nucl. Mater. 179-181 (1991) 771.
[5] H.M. Chung, B.A. Loomis, D.L. Smith, J. Nucl. Mater. 212–215 (1994) 804.
[6] D.L. Smith, H.M. Chung, H. Matsui, A.F. Rowcliffe, Fusion Eng. Des. 41 (1998) 7.
[7] D.L. Smith, M.C. Billone, K. Natesan, Int. J. Refract. Met. Hard Mater. 18 (2000) 213.
[8] N. Baluc, Phys. Scr. T138 (2009) 014004.
[9] T. Nagasaka, N.J. Heo, T. Muroga, M. Imamura, Fusion Eng. Des. 61 (62) (2002) 757.
[10] D.L. Smith, H.M. Chung, B.A. Loomis, H.C. Tsai, J. Nucl. Mater. 233-237 (1996) 356.
[11] D.R. Diercks, B.A. Loomis, J. Nucl. Mater. 141-143 (1986) 1117.
[12] B. Zhu, S. Yang, M. Zhang, J. Ding, Y. Long, F. Wan, Mater. Charact. 111 (2016) 60.

[13] M. Hatakeyama, T. Muroga, S. Tamura, I. Yamagata, J. Nucl. Mater. 417 (2011) 303.
[14] J.M. Chen, T. Muroga, T. Nagasaka, Y. Xu, C. Li, S.Y. Qiu, Y. Chen, J. Nucl. Mater. 334 (2004) 159.
[15] T. Muroga, T. Nagasaka, P.F. Zheng, J.M. Chen, Adv. Sci. Technol. 73 (2010) 22.
[16] M.S. Staltsov, I.I. Chernov, B.A. Kalin, K.Z. Oo, A.A. Polyansky, O.S. Staltsova, et al., J. Nucl. Mater. 461 (2015) 56.
[17] A. van Veen, A.V. Fedorov, A.I. Ryazanov, J. Nucl. Mater. 258-263 (1998) 1400.
[18] P. Hartel, H. Rose, C. Dignes, Ultramicroscopy 63 (1996) 93.
[19] R.F. Egerton, Electron Energy-Loss Spectroscopy in the Electron Microscope, Springer, 2011.
[20] E. Stoyanov, F. Langenhorst, G. Steinle-Neumann, Am. Mineral. 92 (2007) 577.
[21] N.G. Alexandropoulos, G. Bambakidis, T. Sparrow, B. Williams, J. Phys. F: Met. Phys. 16 (1986) L24S.
[22] M.D. Banus, T.B. Reed, A.J. Strauss, Phys. Rev. B 5 (1972) 2775.
[23] A.I. Gusev, J. Exp. Theor. Phys. 117 (2013) 293.
[24] H.O. Pierson, Handbook of Refractory Carbides and Nitrides: Properties, Characteristics, Processing, and Applications, Noyes Publications, 1996.
[25] R.W. Powers, M.V. Doyle, Acta Metall. 6 (1958) 643.
[26] R.W. Powers, M.V. Doyle, J. Appl. Phys. 30 (1959) 514.
[27] H. Nakajima, S. Nagata, H. Matsui, S. Yamaguchi, Philos. Mag. 67 (1993) 557.
[28] J.F. Murdock, C.J. McHargue, Acta Metall. 16 (1968) 493.
[29] R.E. Howard, Phys. Rev. 144 (1966) 650.
[30] R.E. Howard, A.B. Lidiard, Rep. Prog. Phys. 27 (1964) 161.
[31] Y. Liu, Y. Ge, T. Pan, L. Zhang, J. Alloys Compd. 470 (2009) 176.
[32] M.J. Demkowicz, P. Bellon, B.D. Wirth, MRS Bull. 35 (2010) 992.
[33] J. Laakmann, P. Jung, W. Uelhoff, Acta Metall. 35 (1987) 2063.
[34] F. Gao, H. Heinisch, R.J. Kurtz, J. Nucl. Mater. 351 (2006) 133.
[35] M.J. Demkowicz, A. Misra, A. Caro, Curr. Opin. Solid State Mater. Sci. 16 (2012) 101.
[36] P.D. Edmonson, C.M. Parish, Y. Zhang, A. Hallén, M.K. Miller, Scr. Mater. 65 (2011) 731.
[37] Y. Wu, J. Ciston, S. Kräemer, N. Bailey, G.R. Odette, P. Hosemann, Acta Mater. 111 (2016) 108.
[38] E.G. Fu, A. Misra, H. Wang, L. Shao, X. Zhang, J. Nucl. Mater. 407 (2010) 178.